Gas-driven subcritical crack propagation during the conversion of oil to gas

Z. Q. Fan[1], Z.-H. Jin[1*] and S. E. Johnson[2]

[1]*Department of Mechanical Engineering, University of Maine, Orono, ME 04469, USA*
[2]*Department of Earth Sciences, University of Maine, Orono, ME 04469, USA*
**Corresponding author (e-mail: zhihe.jin@maine.edu)*

ABSTRACT: In this paper, we investigate subcritical propagation of an initially oil-filled, sub-horizontal microcrack driven by the excess fluid pressure associated with the conversion of oil to gas in a petroleum source rock under continuous burial. The crack propagation distance and propagation duration (the time required for the crack to propagate during conversion of all oil to gas), as well as the excess pressure inside the crack, are determined using a finite difference scheme that couples linear elastic fracture mechanics, oil–gas transformation kinetics and an equation of state for the gas. The effects of the source-rock temperature at the initial depth of the microcrack and fracture properties of the source rock are also considered. Our numerical results show that higher burial rates significantly reduce the crack propagation duration. However, the influence of the geothermal gradient on the propagation duration and distance is only marginal. Similar to the results for the oil-driven crack propagation during kerogen–oil conversion, the duration of gas-driven crack propagation is also governed by transformation kinetics because the subcritical crack propagation rate is much faster than the oil–gas conversion rate.

INTRODUCTION

Kerogen derived from organic material deposited in sedimentary basins releases hydrocarbons after a succession of chemical transformations. In general, the hydrocarbon generation process consists of three stages, described as follows (Hunt 1979; Tissot & Welte 1984; Tissot *et al*. 1987; Luo & Vasseur 1996; Hantschel & Kauerauf 2009). In the first stage, the organic material undergoes progressive burial to form kerogen. Although microbial processes lead to some gas generation, the gas is difficult to accumulate during this stage due to the poor preservation conditions at shallow burial depth. With increasing burial depth, increasing temperature reaches a threshold value where kerogen begins to release hydrocarbons. This is the principal stage of oil generation. The conversion of kerogen to oil is accompanied by the formation of a moderate to significant amount of gas depending on the type(s) of kerogen (Tissot & Welte 1984; Cornford 1998). In the final stage, as the temperature continues to increase, large amounts of gas are generated from the thermal cracking of oil, with >90% of the gas being methane (Berg & Gangi 1999). At the end of the evolution, the final products are gas and bitumen/graphite residue.

Associated with the conversion of kerogen to oil and/or gas, volume increases significantly due to the density difference between the precursor and the product. For the transformation of kerogen to oil, the volume expansion is about 10–20% (Ozkaya 1988), which is high enough to fracture the host rock and cause subcritical propagation of oil-filled cracks (Lash & Engelder 2005, 2009; Fan *et al*. 2010; Jin *et al*. 2010). For the conversion of oil to gas, Barker (1990) performed a calculation on the volume change and found that extremely high pressure develops as oil converts to gas under subsurface conditions, which may further grow the oil-filled cracks. Horsfield *et al*. (1992) simulated the conversion of oil to gas using pyrolysis experiments and compared the simulation results with observed petroleum reservoir data. Wang *et al*. (2007) modelled oil–gas conversion and identified some controlling parameters for gas expulsion and accumulation under specific geological conditions. Guo *et al*. (2009) compared gases derived from kerogen and oil, and proposed an approach to differentiate gases from different sources based on chemical compositions. Stainforth (2009) compared the available studies on petroleum generation and migration and proposed a new model to predict petroleum expulsion. Luo (2010) proposed a fault-controlling hydrocarbon hypothesis and showed the potential application in hydrocarbon generation and exploration. Lewan & Roy (2011) discussed the role of water in petroleum generation from kerogen.

Although the dominant mechanism for hydrocarbon expulsion and migration from the source rock to the reservoir is still in debate, fracture-induced permeability is commonly cited as the most likely mechanism for primary migration out of source rocks which are characterized by extremely low permeability and porosity (e.g. Palciauskas & Domenico 1980; Comer & Hinch 1987; England *et al*. 1987; Hunt 1990; Miller 1995; Nunn 1996; Law & Spencer 1998; Nelson 2001; Lash & Engelder 2005, 2009; Jin & Johnson 2008; Fan *et al*. 2010). Microcracks induced by the excess oil/gas pressure may propagate and form an interconnected fracture network acting as hydrocarbon migration pathways. Capuano (1993) observed horizontal microfractures filled with calcium sulfate and organic materials at depths of about 3–5 km in geopressured shales from the Oligocene Frio Formation of the Texas Gulf Coast. Marquez & Mountjoy (1996) found horizontal microcracks at depths of 3.8–5 km in the deep Alberta basin and concluded that the microcracks form

Petroleum Geoscience, Vol. **18**, 2012, pp. 191–199
DOI: 10.1144/1354-079311-030.

as a result of oil–gas conversion. Lash & Engelder (2005) found bitumen-filled horizontal microcracks in the Upper Devonian Dunkirk Shale, western New York State indicating possible hydrocarbon migration through microcracks in black shale formations.

Many field and computational investigations have been conducted to correlate microcrack development and hydrocarbon generation. Palciauskas & Domenico (1980) calculated the depths for the onset of microcracking in overpressured sedimentary rocks undergoing burial. Bredehoeft *et al*. (1994) simulated microfracture initiation resulting from overpressure caused by oil generation and discussed the effect of fracture-induced permeability on the migration of oil. Vernik (1994) found bedding-parallel microcracks in source rocks and estimated the excess oil pressure available to initiate critical crack propagation. Berg & Gangi (1999) modelled the pressure change and fracture initiation caused by oil generation. Carcione & Gangi (2000) considered the overpressure development induced by the oil–gas transformation. Lash & Engelder (2005) carried out extensive studies on horizontal microcracks in finely laminated black shale. They analysed the state of stresses around the microcracks and suggested that horizontal microcracks initiate as a result of strength anisotropy, imposed in part from kerogen particle orientation. Jin *et al*. (2010) and Fan *et al*. (2010) investigated subcritical propagation and coalescence of oil-filled microcracks during conversion of kerogen to oil. They showed that the rate of excess pressure buildup from kerogen–oil conversion is not fast enough to drive critical growth of the microcracks. They also showed that a penny-shaped crack initiating from a flat kerogen particle may grow to more than five times its original diameter if all kerogen is converted to oil.

The oil contained in the microcracks converts to gas when the temperature enters the gas window at deeper burial depths in source rocks. The excess pressure resulting from the volume increase associated with oil–gas conversion may further drive the crack to grow, thereby increasing the chance of forming interconnected fracture networks. The crack growth process may take millions of years when the oil has been completely converted to gas. A quantitative description of the process is thus crucial to the understanding of hydrocarbon expulsion and migration. Nunn & Meulbroek (2002) evaluated the vertical migration of hydrocarbons through critical propagation of a methane-filled fracture. They assumed that the fracture was always filled with methane gas and did not consider the oil–gas conversion.

In this paper, we investigate microcrack propagation driven by the excess fluid pressure accompanying the oil–gas conversion during burial of the hydrocarbon. A penny-shaped crack is considered since it has typically been observed in sedimentary rocks (Lacazette & Engelder 1992; Savalli & Engelder 2005; Olson 1993). We assume that the crack is initially filled with oil in a linearly elastic source rock of essentially zero permeability and the final state is a gas-filled crack when all the oil has been converted to gas. The source rock may not behave elastically during the entire history of oil–gas conversion (typically on the order of 10^6 years). However, the linear elastic assumption may still be used as we will see that crack propagation is governed by oil–gas transformation kinetics. Oil compressibility is not considered as its effect is overshadowed by the much higher gas compressibility. For example, the typical value for oil compressibility is 1.5×10^{-5} psi^{-1} (Berg & Gangi 1999). Therefore, a 1.0 MPa pressure change will result in a 0.2% oil volume change, which can be ignored during crack propagation. We first derive a finite difference formulation to simulate subcritical crack propagation during oil–gas conversion. The coupled processes of oil–gas conversion, compression of the gas and crack propagation are included in the model. Numerical results are presented to illustrate the effects of burial rate, geothermal gradient, temperature at the initial crack location and fracture toughness of the source rocks on the propagation behaviour of oil/gas-filled cracks, including propagation distance and duration (the time required for the crack to propagate during conversion of all oil to gas).

THEORETICAL FORMULATION OF SUBCRITICAL CRACK PROPAGATION DUE TO GAS GENERATION

Oil–gas transformation kinetics

The conversion of oil to gas is generally described by the following transformation kinetics (Tissot & Welte 1984; Pepper & Dodd 1995; Berg & Gangi 1999)

$$\frac{dM}{dt} = -kM, \tag{1}$$

where M is the mass of convertible oil, t is time and k is the reaction rate which follows the Arrhenius law

$$k = B\exp\left[-\frac{E_A}{RT(t)}\right]. \tag{2}$$

In the above equation, B is a pre-exponential constant, E_A is the activation energy of the transformation, R is the universal gas constant, and T is the absolute temperature. T varies with time during burial as both burial rate and geothermal gradient influence the hydrocarbon temperature. For burial depths in the typical range of 3–6 km, a linear geothermal gradient may be used. Moreover, we also adopt the assumption of a constant burial rate following Berg & Gangi (1999). The hydrocarbon temperature may thus be expressed by

$$T(t) = T_0 + G(z - H_0) \tag{3}$$

where H_0 is the initial burial depth at which the oil-filled crack is located, T_0 is the temperature at H_0, G is the geothermal gradient, and z is the burial depth given by

$$z = H_0 + St, \tag{4}$$

where S is the burial rate. Substituting equation (4) into equation (3) produces the hydrocarbon temperature as follows:

$$T(t) = T_0 + GSt. \tag{5}$$

For practical applications, the parameters G, S, T_0 and H_0 need to be selected so that the gas window falls in the temperature range determined from equation (5).

Oil mass at time t during the conversion can be obtained by integration of equation (1) as follows:

$$M = M_0\exp\left[-\Phi(t)\right], \tag{6}$$

where M_0 is the initial oil mass and $\Phi(t)$ is given by:

$$\Phi(t)=\frac{B(T_0+GSt)}{GS}\exp\left[-\frac{E_A}{R(T_0+GSt)}\right]-\frac{BT_0}{GS}\exp\left(-\frac{E_A}{RT_0}\right)+\frac{BE_A}{RGS}\left[E_i\left(-\frac{E_A}{R(T_0+GSt)}\right)-E_i\left(-\frac{E_A}{RT_0}\right)\right] \quad (7)$$

in which $E_i(\ )$ is the exponential integral defined by

$$E_i(x)=\int_{-\infty}^{x}\frac{e^{x'}}{x'}dx'.$$

The mass and volume of the gas are now given by

$$M_{gas}=M_0-M=M_0\left[1-\exp\left[-\Phi(t)\right]\right] \quad (8a)$$

$$V_{gas}=M_0\left[1-\exp\left[-\Phi(t)\right]\right]/\rho_{gas}, \quad (8b)$$

where ρ_{gas} is the gas density. The volume of oil is given by

$$V_{oil}=M_0\exp\left[-\Phi(t)\right]/\rho_{oil}, \quad (9)$$

where ρ_{oil} is the density of oil.

Equation of state for gas

At high temperatures and pressures, gas behaviour deviates from that of the ideal gas. We use an equation of state for methane gas developed by Duan *et al*. (1992) as methane is the prime component of natural gas. The *P–v–T* relation in their model includes a relatively large number of variables, but is applicable across a broad range of temperature and pressure (0–1000 °C and 0–800 MPa, respectively). The equation of state (EOS) for methane gas in the model of Duan *et al*. (1992) is expressed as

$$\frac{P_rV_r}{T_r}=1+\frac{C_1}{V_r}+\frac{C_2}{V_r^2}+\frac{C_3}{V_r^4}+\frac{C_4}{V_r^5}+\frac{C_5}{V_r^2}\left(\beta+\frac{\gamma}{V_r^2}\right)\exp\left(-\frac{\gamma}{V_r^2}\right) \quad (10)$$

where

$$P_r=\frac{P}{P_c},\ T_r=\frac{T}{T_c},\ V_r=\frac{V}{V_c},\ C_1=a_1+\frac{a_2}{T_r^2}+\frac{a_3}{T_r^3},\ C_2=a_4+\frac{a_5}{T_r^2}+\frac{a_6}{T_r^3}.$$

$$C_3=a_7+\frac{a_8}{T_r^2}+\frac{a_9}{T_r^3},\ C_4=a_{10}+\frac{a_{11}}{T_r^2}+\frac{a_{12}}{T_r^3}\ \text{and}\ C_5=\frac{\alpha}{T_r^3}$$

in which P and T are the pressure and temperature of the gas, respectively, T_c is the critical temperature above which methane cannot be liquefied no matter what pressure is applied, P_c is the critical pressure required to liquefy methane at the critical temperature T_c, V_c is related to P_c and T_c by

$$V_c=\frac{RT_c}{P_c}, \quad (11)$$

and V is the molar volume given by

$$V=\frac{m}{\rho_{gas}}, \quad (12)$$

where m is the molar mass. In the above equations, a_i (i = 1, 2, . . ., 12), α, β and γ are material constants which can be found in Duan *et al*. (1992).

The gas pressure can be expressed in terms of gas density using equation (10) as follows

$$P=P(\rho_{gas})=\frac{P_cT_rV_c\rho_{gas}}{m}\left[1+\frac{BV_c\rho_{gas}}{m}+\frac{CV_c^2\rho_{gas}^2}{m^2}+\frac{DV_c^4\rho_{gas}^4}{m^4}+\frac{EV_c^5\rho_{gas}^5}{m^5}+\frac{FV_c^2\rho_{gas}^2}{m^2}\left(\beta+\frac{\gamma V_c^2\rho_{gas}^2}{m^2}\right)\exp\left(-\frac{\gamma V_c^2\rho_{gas}^2}{m^2}\right)\right]. \quad (13)$$

Using equations (12) and (13), we can calculate the density of methane gas as a function of pressure and temperature. Figure 1 shows the density as a function of pressure for various temperatures ranging from 100–200 °C. The gas density increases with increasing pressure and decreasing temperature as expected. We note that the *P–v–T* relation and the calculated density for natural gas may be very sensitive to the gas composition and the calculations based on the EOS for methane are first-order approximations.

Linear elastic fracture mechanics model

We first consider a sub-horizontal, layer-parallel, penny-shaped crack, as shown in Figure 2. The crack of radius a_0 is initially filled with oil. The initial excess oil pressure is denoted by Δp_0 (fluid pressure beyond the overburden pressure, Engelder & Lacazette 1990). For layer-parallel cracks the loading is dominantly symmetrical about the crack plane. We thus neglect the effect of any shear stress on the crack initiation and propagation. Crack propagation will be initiated due to the excess fluid pressure resulting from the oil–gas conversion. At time t, the excess pressure on the crack surface Δp is given by

$$\Delta p=P(\rho_{gas})-\rho_s gz=P(\rho_{gas})-\rho_s g(H_0+St) \quad (14)$$

where ρ_s is the average sediment density, g = 9.8 m s^{-2} is the gravitational acceleration, and $P(\rho_{gas})$ is the gas pressure given by equation (13). We note that gas pressure in the crack is not the usual pore pressure of the host rock which is assumed here to have

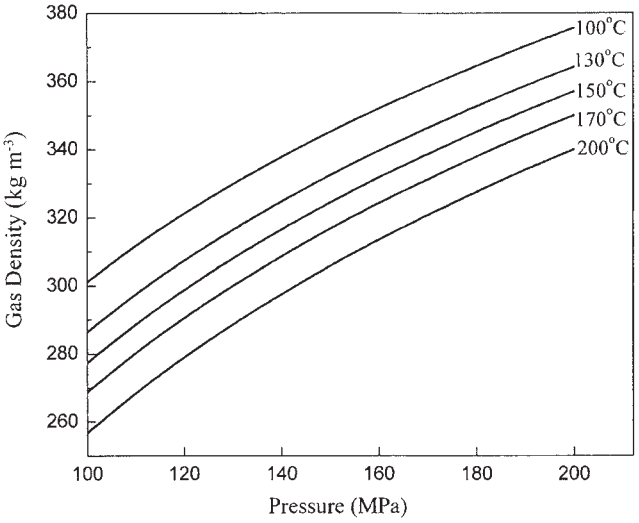

Fig. 1. Density of methane as a function of temperature and pressure using the equation of state given by Duan *et al*. (1992).

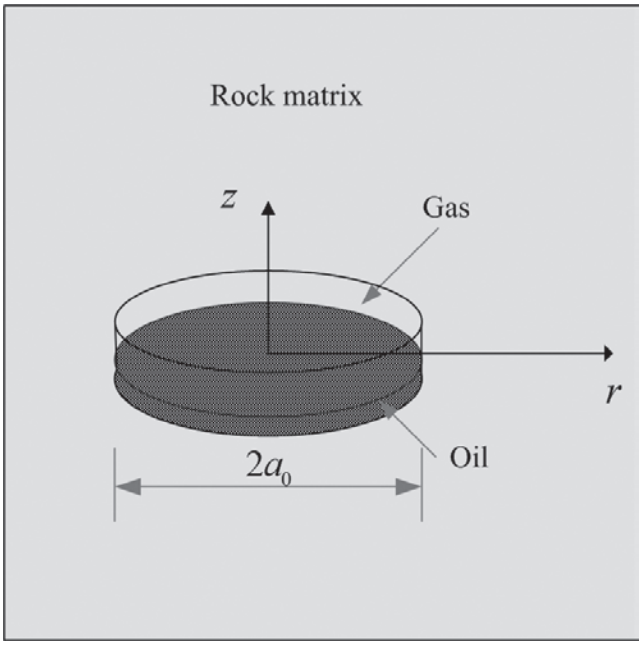

Fig. 2. Schematic illustration of an oil/gas-filled penny-shaped microcrack in a source rock.

zero permeability. The pore pressure develops when the microcracks coalesce to form a fracture network in the source rock.

The stress intensity factor along the crack front can be found in Tada *et al*. (2000) and it is given by

$$K_{\mathrm{I}} = 2\Delta p\sqrt{a_0/\pi}. \tag{15}$$

The volume of the crack is

$$V_{\mathrm{crack}} = \frac{16(1-\nu^2)\Delta p}{3E}a_0^3, \tag{16}$$

where E and ν are Young's modulus and Poisson's ratio of the host rock, respectively. The initial oil mass is thus given by

$$M_0 = \frac{16(1-\nu^2)a_0^3\Delta p_0}{3E}\rho_{\mathrm{oil}}. \tag{17}$$

Critical crack propagation takes place if the stress intensity factor K_{I} in equation (15) reaches the fracture toughness K_{Ic} of the host rock. On the other hand, subcritical crack propagation occurs in the rock when the stress intensity factor K_{I} has not reached K_{Ic} but exceeds the threshold value K_{Ith}, which is usually a fraction (e.g. 20–50%) of K_{Ic}. Our investigations into the propagation of sub-horizontal cracks during kerogen–oil conversion (Fan *et al*. 2010; Jin *et al*. 2010) showed that hydrocarbon generation usually induces subcritical crack propagation because the rate of excess pressure build-up from kerogen–oil conversion is not fast enough to drive critical growth of the microcracks. Several mechanisms are responsible for subcritical crack growth in rocks, including chemical reaction between the rocks and their local environment, presence of stress corrosion agents, and diffusion (Atkinson 1984; Freiman 1984; Freiman *et al*. 2009). In general, the subcritical crack propagation velocity, v, can be related to the stress intensity factor according to the Charles law (Atkinson 1984; Freiman 1984)

$$v = \frac{da}{dt} = A\left[K_{\mathrm{I}}(a)\right]^n, \tag{18}$$

where A and n are material constants.

Equating K_{I} in equation (15) to K_{Ith}, we obtain the excess pressure corresponding to the onset of subcritical crack propagation as follows

$$\Delta p_{\mathrm{th}} = K_{\mathrm{Ith}}\sqrt{\pi}/(2\sqrt{a_0}). \tag{19}$$

The corresponding crack volume is determined as

$$V^0_{\mathrm{crack}} = \frac{16(1-\nu^2)a_0^3}{3E}\Delta p_{\mathrm{th}}. \tag{20}$$

As the crack is filled by both oil and gas during propagation, the volume of the crack is equal to the sum of oil and gas volumes if we neglect the mutual solubility of gas and oil, i.e.

$$V^t_{\mathrm{oil}} + V^t_{\mathrm{gas}} = V^t_{\mathrm{crack}}, \tag{21}$$

where V^t_{crack}, V^t_{oil} and V^t_{gas} are the crack, oil and gas volumes at time t, respectively. Combining equations (8), (9), (13), (19), (20) and (21) gives the following two equations to determine t_0, the time period from the start of oil–gas conversion to the moment that the stress intensity factor reaches K_{Ith}, and the corresponding gas density $\rho^{\mathrm{th}}_{\mathrm{gas}}$.

$$P\left(\rho^{\mathrm{th}}_{\mathrm{gas}}\right) - \rho_{\mathrm{s}}g(H_0 + St_0) = K_{\mathrm{Ith}}\sqrt{\pi}/\left(2\sqrt{a_0}\right) \tag{22a}$$

$$\frac{M_0\left[1-\exp\left[-\Phi(t_0)\right]\right]}{\rho^{th}_{gas}} + \frac{M_0\exp\left[-\Phi(t_0)\right]}{\rho_{oil}} = \frac{16(1-\nu^2)a_0^3}{3E}\frac{K_{Ith}\sqrt{\pi}}{2\sqrt{a_0}}. \tag{22b}$$

Finite difference simulation of subcritical crack propagation

A finite difference scheme is adopted to simulate the subcritical propagation of the oil/gas-filled penny-shaped crack. Consider subcritical crack propagation from time t_0 to the current time t. We partition the time domain $t - t_0$ using a mesh t_0, t_1,. . ., $t_{\mathrm{N-1}}$, t_{N}. The radius of the crack at step t_{i} is denoted by a_{i} and the corresponding gas density is ρ^i_{gas}. Using a forward difference at time t_{i} to approximate the first derivative in equation (18), we can obtain the crack radius at $t_{\mathrm{i+1}}$ as follows

$$a_{i+1} = a_i + A[P(\rho^i_{\mathrm{gas}}) - \rho_{\mathrm{s}}g(H_0 + St_i)]^n(a_i)^{n/2}\left[2/\sqrt{\pi}\right]^n(t_{i+1} - t_i). \tag{23}$$

The oil volume at $t_{\mathrm{i+1}}$ is determined by

$$V^{i+1}_{\mathrm{oil}} = \frac{M_0\exp\left[-\Phi(t_{i+1})\right]}{\rho_{\mathrm{oil}}}. \tag{24}$$

Here we ignore the compressibility of oil and hence the oil density remains constant. The gas volume at $t_{\mathrm{i+1}}$ is given by

$$V^{i+1}_{\mathrm{gas}} = \frac{M_0[1-\exp\left(-\Phi(t_{i+1})\right)]}{\rho^{i+1}_{\mathrm{gas}}}, \tag{25}$$

where ρ_{gas}^{i+1} is the gas density at step t_{i+1}. The volume of the crack at t_{i+1} is

$$V_{crack}^{i+1} = \frac{16(1-\nu^2)\Delta p_{i+1}}{3E} a_{i+1}^3, \tag{26}$$

where $\Delta p_{i+1} = P(\rho_{gas}^{i+1}) - \rho_s g\left(H_0 + St_{i+1}\right)$ is the excess pressure at step t_{i+1}. Setting the above volume equal to the sum of the oil and gas volume at t_{i+1}, we obtain the excess pressure Δp_{i+1} at t_{i+1} as follows

$$\Delta p_{i+1} = \left[\frac{M_0 \exp\left(-\Phi\left(t_{i+1}\right)\right)}{\rho_{oil}} + \frac{M_0[1-\exp\left(-\Phi\left(t_{i+1}\right)\right)]}{\rho_{gas}^{i+1}}\right] \Bigg/ \left[\frac{16(1-\nu^2)}{3E} a_{i+1}^3\right] \tag{27}$$

or

$$P(\rho_{gas}^{i+1}) - \rho_s g\left(H_0 + St_{i+1}\right) = \left[\frac{M_0 \exp\left(-\Phi\left(t_{i+1}\right)\right)}{\rho_{oil}} + \frac{M_0[1-\exp\left(-\Phi\left(t_{i+1}\right)\right)]}{\rho_{gas}^{i+1}}\right] \Bigg/ \left[\frac{16(1-\nu^2)}{3E} a_{i+1}^3\right], \tag{28}$$

where $P(\rho_{gas}^{i+1})$ can be determined from equation (13). Solving equation (28) for the unknown gas density ρ_{gas}^{i+1}, the excess pressure Δp_{i+1} at t_{i+1} can be obtained using equation (27). For the microcrack to propagate subcritically, Δp_{i+1} must satisfy the following condition so that the stress intensity factor at the crack tip is equal to or greater than the threshold value K_{Ith}; that is

$$\Delta p_{i+1} \geq \frac{K_{Ith}}{2\sqrt{a_{i+1}/\pi}}. \tag{29}$$

If the above condition is not satisfied, which means there has not been sufficient amount of gas converted from oil and the excess pressure is not high enough to drive subcritical crack propagation, time t_{i+1} should be determined by solving equation (22) with a_0, t_0 and ρ_{gas}^{th} replaced by a_{i+1}, t_{i+1} and ρ_{gas}^{i+1}, respectively.

NUMERICAL RESULTS AND DISCUSSIONS

This section presents numerical examples to illustrate the effects of geothermal gradient, burial rate, source-rock temperature at the initial crack location, and fracture properties of the source rock on the gas-driven crack propagation behavior, including crack propagation distance and excess fluid pressure in the crack. The propagation distance of an oil/gas-filled crack is a key quantity to understand hydrocarbon migration through fracture propagation. The excess fluid pressure is a driving force for crack propagation and hence hydrocarbon migration. Our model is applicable to sedimentary basins in general and the host rock is treated as a linear elastic solid with general characteristics of black shale formations. The base parameters used in the numerical calculation are listed in Table 1. The material properties are for typical shales (see, for example, Luo & Vasseur 1996; Nunn 1996; Berg & Gandi 1999). Our previous studies on subcritical growth of oil-filled cracks during kerogen–oil conversion (Fan *et al*. 2010; Jin *et al*. 2010) indicate that the crack growth rate is governed by transformation kinetics because the subcritical crack propagation rate according to the Charles law (equation 18) is much faster than the oil–gas conversion rate. As a result, the subcritical crack growth parameters A and n in equation (18) are effectively irrelevant and only the subcritical crack growth velocity at $K_I = K_{Ith}$ plays a role in determining the crack propagation rate and duration (the crack will not grow if the stress intensity factor is smaller than K_{Ith}). A and n can thus be selected somewhat arbitrarily and, in this study, we choose $A = 10^7$ m s^{-1} (MPa-m$^{1/2}$)$^{-n}$ and $n = 10$. The resulting crack propagation velocities are 10^{-10} m s^{-1} and 10^{-3} m s^{-1} when the stress intensity factor assumes the selected values of K_{Ith} and K_{Ic}, respectively, which are consistent with typical subcritical crack propagation velocities in the range of 10^{-10} to 10^{-2} m s^{-1} (Atkinson 1984; Freiman 1984).

Table 1. *Physical and geometrical parameters used in the model*

Symbols	Definition	Value (unit)
Rock matrix		
E	Young's modulus	2.0 GPa
ν	Poison's ratio	0.4
ρ_s	Average sediment density	2350 kg m^{-1}
A	Subcritical crack growth constant	10^7 m s^{-1} (MPa-m$^{1/2}$)$^{-10}$
n	Subcritical crack growth index	10
a_0	Initial microcrack radius	50 μm
H_0	Initial depth	4000 m
Oil		
ρ_{oil}	Oil density	850 kg m^{-3}
Methane		
m	Molar mass	16 g mol^{-1}
T_c	Critical temperature	191.1 K
P_c	Critical pressure	4.64 MPa
Kinetics		
B	Pre-exponential constant	1.744×10^{13} s^{-1}
R	Universal gas constant	8.314 J mole^{-1} K^{-1}
E_A	Activation energy	217.6 kJ mol^{-1}

In our parametric analyses, the geothermal gradient varies from 20–40 °C km^{-1} (Berg & Gandi 1999), burial rate varies from 0.05–0.2 km Ma^{-1} (Carcione & Gangi 2000) and the threshold stress intensity factor K_{Ith} varies from 0.02–0.2 MPa-m$^{1/2}$ (accordingly the fracture toughness of the host rock varies from 0.1–1.0 MPa-m$^{1/2}$ (Atkinson 1984; Nunn 1996) with the assumption of $K_{Ith} = 0.2K_{Ic}$). It is noted that some combinations of the above burial rates and geothermal gradients may yield a relatively higher heating rate (e.g. 40 °C km^{-1} geothermal gradient with 0.2 km Ma^{-1} burial rate). We choose these parameters from Berg & Gangi (1999) and include them in the numerical calculations just for the purpose of sensitivity analysis. Moreover the geothermal gradient is assumed to be independent of burial rate and thermal capacity of the sediment. We also examine the sensitivity of subcritical propagation distance and duration to the temperature at the initial crack location in the range of 140–160 °C. The initial crack is assumed to form at a depth of $H_0 = 4$ km.

We assume that at the initial crack length, the stress intensity factor equals the threshold value K_{Ith} due to excess oil pressure. This state can be regarded as the end state of crack propagation due to kerogen–oil conversion (Fan *et al*. 2010; Jin *et al*. 2010). Hence, the initial excess oil pressure is taken as $\Delta p_0 = \Delta p_{th}$ given in equation (20).

Figures 3 and 4 show the normalized crack length and the excess pressure, respectively, versus time for various geothermal gradients. The following parameters are used in the computation: threshold stress intensity factor $K_{Ith} = 0.02$ MPa-m$^{1/2}$ ($K_{Ic} = 0.1$ MPa-m$^{1/2}$), burial rate $S = 0.1$ km Ma^{-1}, and the temperature at the initial crack location $T_0 = 160$ °C. It is seen from the figures that the crack radius increases continuously with time, and the excess pressure decreases continuously during the conversion of

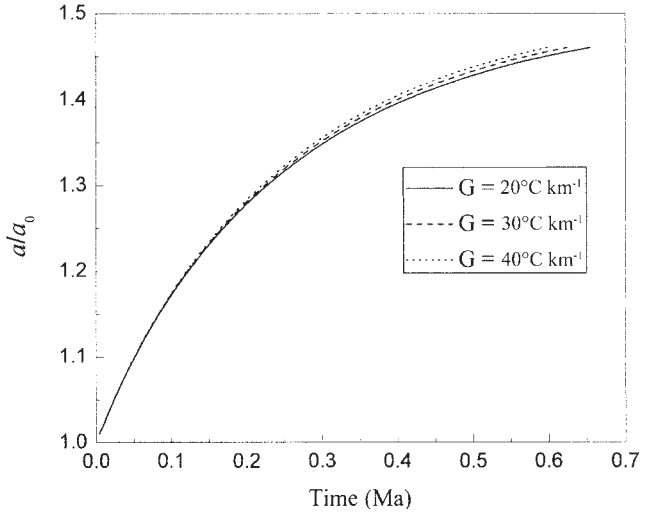

Fig. 3. Effect of geothermal gradient on the propagation distance of an oil/gas-filled microcrack at an initial depth of 4 km under a burial rate of 0.1 km Ma^{-1}.

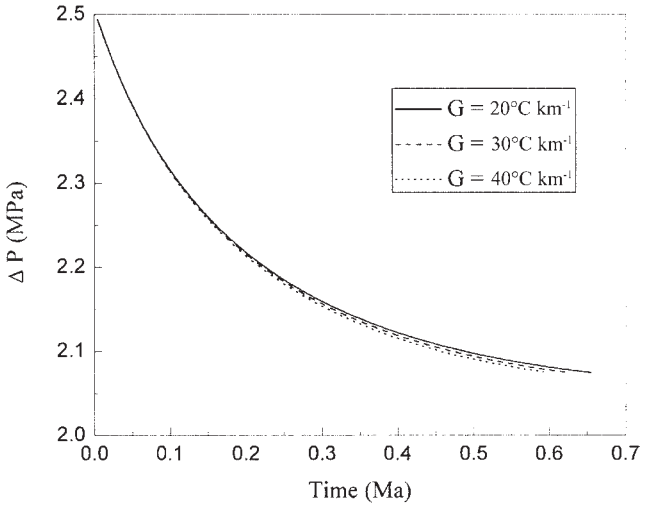

Fig. 4. Effect of geothermal gradient on the excess fluid pressure evolution with time for a microcrack at an initial depth of 4 km under a burial rate of 0.1 km Ma^{-1}.

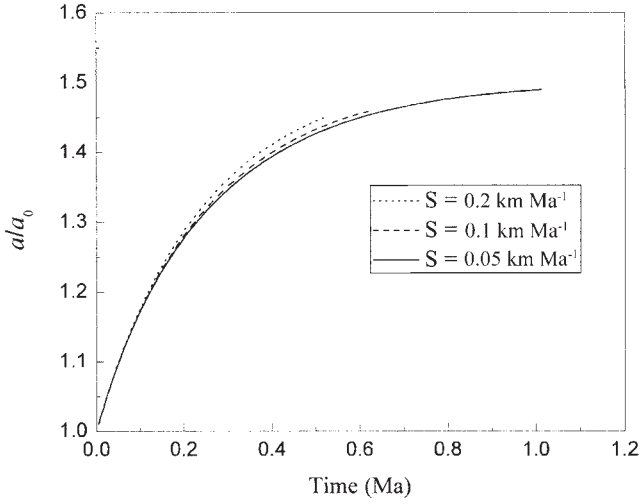

Fig. 5. Effect of burial rate on the crack propagation distance through time for a microcrack at an initial depth of 4 km with a geothermal gradient of 30 °C km^{-1}.

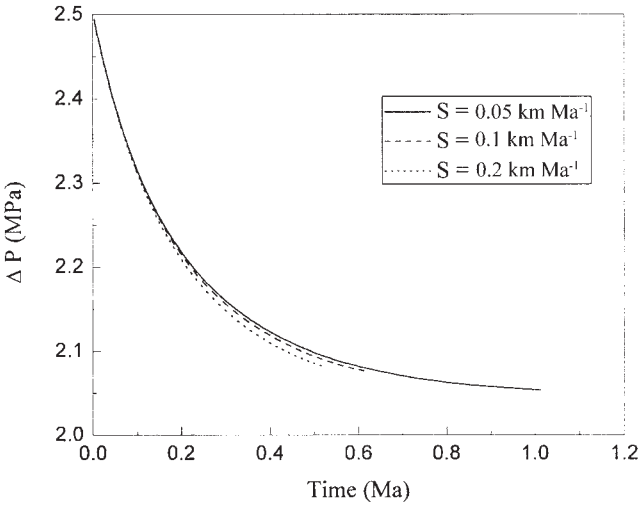

Fig. 6. Effect of burial rate on the excess fluid pressure evolution with time for a microcrack at an initial depth of 4 km with a geothermal gradient of 30 °C km^{-1}.

oil to gas, despite the gas compressibility. This is because the excess pressure is inversely proportional to the square root of the crack radius (equation (29)) and, therefore, decreases with increasing crack radius as conversion of oil to gas proceeds. At a given time, the crack propagation distance increases slightly and the excess pressure decreases with an increase in the geothermal gradient, indicating insignificant influences of the geothermal gradient. Moreover, the final crack diameter and excess pressure are not particularly sensitive to the geothermal gradient. Equations (2) and (5) indicate that the oil–gas conversion rate increases with increasing geothermal gradient. Therefore, crack propagation duration becomes shorter for a source rock with a steeper geothermal gradient. For example, when the geothermal gradient increases from 20–40 °C km^{-1}, the duration for the crack to propagate from an initial diameter of 100 μm to approximately 146 μm decreases from 0.655 to 0.598 Ma, which corresponds to final burial depths of 4065.5 m and 4059.8 m, respectively, at a burial rate of 0.1 km Ma^{-1} and initial burial depth of 4000 m. Since the subcritical crack propagation rate is much faster than the oil–gas conversion rate, crack propagation duration is governed mainly by the transformation kinetics (of oil-to-gas cracking), which is similar to that for oil-driven crack propagation during the conversion of kerogen to oil (Fan *et al*. 2010; Jin *et al*. 2010).

Fan *et al*. (2010) showed that a penny-shaped crack initiating from a flat kerogen particle of the assumed thickness may grow to more than five times its original diameter if all kerogen is converted to oil. The present example shows that gas generation induces an additional crack propagation distance of one-half the oil crack diameter. Hence, the final crack diameter may reach seven to eight times the original kerogen particle size when all kerogen is eventually converted to gas. The relatively small crack propagation distance from oil–gas conversion is due to the gas compressibility as well as our assumption that the initial crack induced by kerogen–oil conversion has zero thickness but the oil-filled crack has a finite volume at the start of oil–gas conversion.

The effects of the burial rate on the crack propagation distance and excess oil/gas pressure are shown in Figures 5 and 6, respectively. The base material and physical properties are the same as those in Figure 3 but the geothermal gradient is taken as G = 30 °C km^{-1}. Equations (2) and (5) imply that the oil–gas

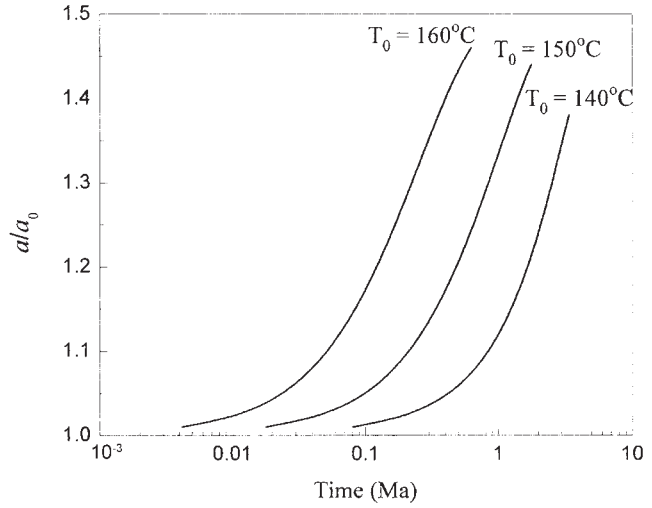

Fig. 7. Effect of the source-rock temperature at the initial crack location on the propagation distance of a microcrack at an initial depth of 4 km with a geothermal gradient of 30 °C km^{-1} and a burial rate of 0.1 km Ma^{-1}.

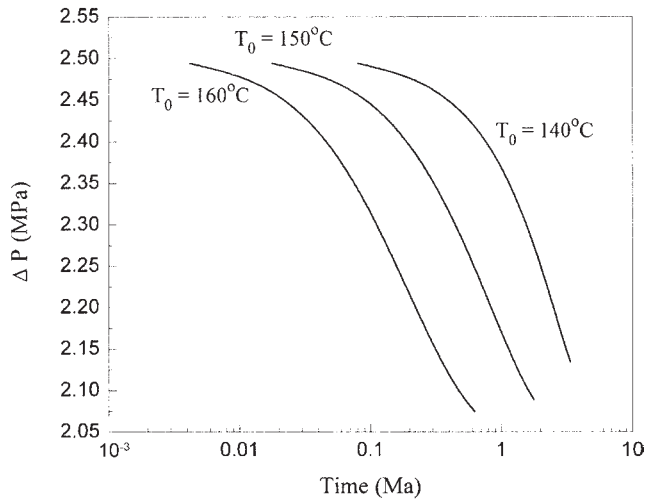

Fig. 8. Effect of the source-rock temperature at the initial crack location on the excess pressure for a microcrack at an initial depth of 4 km with a geothermal gradient of 30 °C km^{-1} and a burial rate of 0.1 km Ma^{-1}.

conversion rate increases with increasing burial rate. A higher burial rate thus leads to shorter crack propagation duration. For example, when the burial rate increases from 0.05 to 0.2 km Ma^{-1}, the crack propagation duration decreases from 0.6 to 0.52 Ma for the crack to grow from an initial diameter of 100 μm to the final diameter of 145 μm. We also note that crack propagation distance increases slightly with decreasing burial rate. Burial rate has a self-competing effect on the crack propagation as both overburden pressure and temperature increase under continuous burial. Increased overburden pressure during burial makes gas density higher whereas the temperature increase makes gas density lower. Higher gas density means more gas is needed to maintain the same crack volume at a given crack radius/excess pressure. Hence, the crack propagation distance becomes shorter. Moreover, the reduced crack propagation duration is caused mainly by the increasing temperature during burial.

Figures 7 and 8 show the effects of the source rock temperature T_0 at the initial crack location on the crack propagation distance and excess oil/gas pressure, respectively. Note that here we assume oil (in the microcrack at a depth of 4 km)

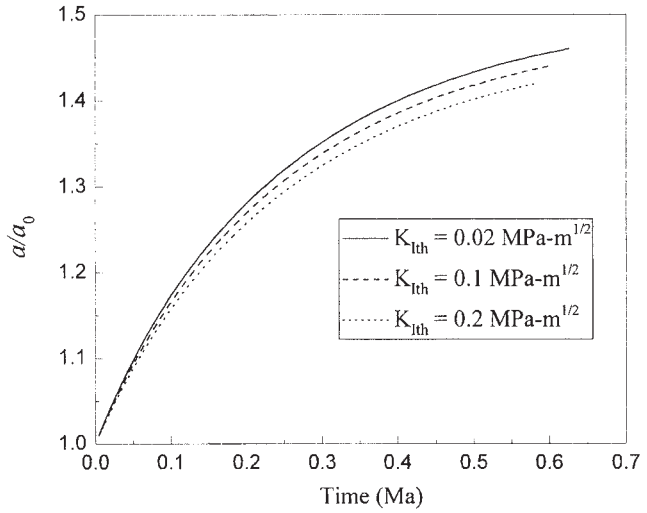

Fig. 9. Effect of fracture toughness of the source rock on the propagation distance of a microcrack at an initial depth of 4 km with a geothermal gradient of 30 °C km^{-1} and a burial rate of 0.1 km Ma^{-1}.

starts to convert to gas at T_0. Other parameters are chosen as follows: geothermal gradient G = 30 °C km^{-1}, threshold stress intensity factor K_{Ith} = 0.02 MPa-m$^{1/2}$ (K_{Ic} = 0.1 MPa-m$^{1/2}$), and burial rate S = 0.1 km Ma^{-1}. Temperature plays a crucial role in the conversion of oil to gas as gas generation is highly sensitive to temperature. Equations (2) and (5) indicate that the oil–gas conversion rate increases significantly with increasing temperature which leads to shorter crack propagation duration for the same increase in crack growth. Figure 7 shows that it takes about 3.39 Ma for the crack to grow from an initial diameter of 100 μm to the final diameter of 138 μm with an initial temperature of T_0 = 140 °C, which is five times longer than that for the 160 °C case (0.62 Ma, as shown in Fig. 7). We also observe that crack propagation distance increases with increasing initial temperature. The final crack diameter increases from 138 to 146 μm when T_0 increases from 140 to 160 °C. The influence of temperature on the excess oil/gas pressure is similar to that for crack propagation during kerogen–oil conversion (Fan *et al.* 2010). At a given time, the excess pressure is lower for a crack initially at a higher temperature T_0. This is because the crack has propagated to a larger radius in the higher temperature source rock, as shown in Figure 7, and hence lower pressure is required to continue to propagate the crack.

Finally, the effects of threshold stress intensity factor K_{Ith} (or fracture toughness as K_{Ith} is a fixed fraction of K_{Ic}) of the source rock on the crack propagation distance and excess pressure within the crack are shown in Figures 9 and 10, respectively, with G =30 °C km^{-1}, S = 0.1 km Ma^{-1} and T_0 = 160 °C. It is clear that for subcritical crack propagation a smaller threshold stress intensity factor (and, therefore, a lower fracture toughness value) results in a larger crack propagation distance and lower excess pressure for propagation. Fracture toughness describes the ability of rocks to resist fracture and higher excess pressure is required to propagate the crack with higher fracture toughness. It is noted that the initial volumes of the oil-filled cracks are different for different threshold stress intensity factors. Substituting equation (19) into equation (20) yields

$$V^0_{\text{crack}} = \frac{8\sqrt{\pi}\left(1-\nu^2\right)a_0^3 K_{Ith}}{3E\sqrt{a_0}}, \tag{30}$$

which indicates that the initial volume is proportional to K_{Ith}.

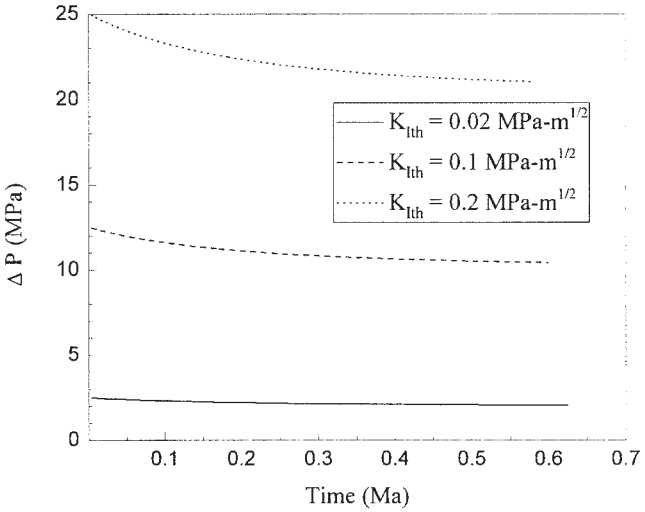

Fig. 10. Effect of fracture toughness of the source rock on the excess pressure evolution with time for a microcrack at an initial depth of 4 km with a geothermal gradient of 30 °C km^{-1} and a burial rate of 0.1 km Ma^{-1}.

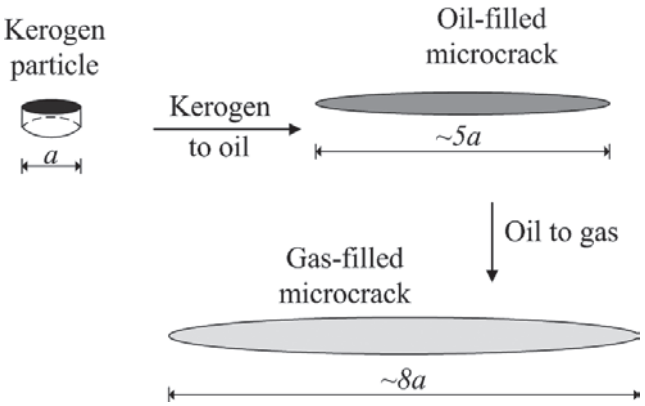

Fig. 11. Schematic illustration of continuous microcrack propagation during the process of kerogen transformation to oil and subsequently oil conversion to gas (modified after Cornford 2011).

CONCLUDING REMARKS

Using linear elastic fracture mechanics, oil–gas transformation kinetics and an equation of state for the gas we have developed a coupled theoretical model to study the subcritical propagation of initially oil-filled, sub-horizontal microcracks during the conversion of oil to gas. The crack propagation distance and duration, and excess oil/gas pressure in the crack are determined. Parametric sensitivity analysis is used to examine the effects of four parameters (geothermal gradient, burial rate, the temperature at the initial crack location, and fracture toughness of the source rock) on the hydrocarbon migration through subcritical crack propagation. From the theoretical model, and the numerical analysis and calculations, we reach a number of conclusions.

1. Microcracks resulting from volume expansion caused by hydrocarbon generation may serve as an effective pathway for primary migration.
2. The excess fluid pressure from gas generation in a sealed system is a significant driving force for subcritical propagation of oil-filled cracks despite gas compressibility. However, the effectiveness of gas generation in driving crack propagation over the time-scale of crack propagation duration needs further investigation as gas may be lost even in rocks of extremely low permeability.
3. Higher burial rates or steeper geothermal gradients shorten the crack propagation duration because of a higher oil–gas conversion rate at higher temperatures but have insignificant effects on the crack propagation distance during continuous burial of hydrocarbons because the propagation distance is determined mainly by the amount of gas generated.
4. Lower fracture toughness (hence lower threshold stress intensity factor) and higher temperature at the initial crack location all yield a larger crack propagation distance, which favours the formation of interconnected networks thus facilitating further migration of oil/gas. Moreover, a higher temperature at the initial crack location yields significantly shorter crack propagation duration. We note that the conclusions on the temperature and fracture toughness effects on the propagation behaviour of penny-shaped cracks are similar to those for oil-driven crack propagation during conversion of solid kerogen to oil (Fan *et al*. 2010).

Our model treats oil and gas as separate phases. Inter-solubility between oil and gas may influence the crack propagation duration but we expect the crack propagation distance will not be changed significantly if all oil is converted to gas. Another limitation of our model is the assumption of zero-permeability for the host rock. All gas converted from oil will thus be available to drive crack propagation. Therefore, the crack propagation distance may be overestimated without consideration of gas leakage. To better understand hydrocarbon migration behaviour, the whole burial history should also be considered so that the increase in pressure and temperature prior to microcrack propagation can be accounted for. We will address these challenging topics in future studies.

The theoretical model and numerical results in Fan *et al*. (2010) suggest that a penny-shaped microcrack forms along the surface of an active flat kerogen particle due to kerogen–oil conversion and may grow to about five times its original diameter driven by the excess pressure generated from the solid–fluid transformation. This paper shows that the crack continues to propagate when the oil in the crack is converted to gas during burial. The final crack diameter may be able to reach about eight times the original kerogen particle size. This process may be summarized by Figure 11.

Acknowledgment is made to the Donors of the American Chemical Society Petroleum Research Fund for support of this research (grant number 47463-AC8). We thank Dr Chris Cornford and an anonymous reviewer for their detailed and insightful comments that led to important improvements.

REFERENCES

Atkinson, B.K. 1984. Subcritical crack growth in geological materials. *Journal of Geophysical Research*, **89**, 4077–4144.

Barker, C. 1990. Calculated volume and pressure changes during the thermal cracking of oil to gas in reservoirs. *American Association of Petroleum Geologists' Bulletin*, **74**, 1254–1261.

Berg, R.R. & Gangi, A.F. 1999. Primary migration by oil-generation microfracturing in low-permeability source rocks: application to the Austin Chalk, Texas. *American Association of Petroleum Geologists' Bulletin*, **83**, 727–756.

Bredehoeft, J.D., Wesley, J.B. & Fouch, T.D. 1994. Simulations of the origin of the fluid pressure, fracture generation, and the movement of fluids in the Unita basin, Utah. *American Association of Petroleum Geologists' Bulletin*, **78**, 1729–1747.

Capuano, R.M. 1993. Evidence of fluid flow in microcracks in geopressured shales. *American Association of Petroleum Geologists' Bulletin*, **77**, 1303–1314.

Carcione, J.M. & Gangi, A.F. 2000. Gas generation and overpressure: Effects on seismic attributes. *Geophysics*, **65**, 1769–1779.

Comer, J.B. & Hinch, H.H. 1987. Recognizing and quantifying expulsion of oil from the Woodford Formation and age-equivalent rocks in Oklahoma and Arkansas. *American Association of Petroleum Geologists' Bulletin*, **71**, 844–858.

Cornford, C. 1998. Source rocks and hydrocarbons of the North Sea. In: Glennie, K.W. (ed.) *Petroleum Geology of the North Sea*. Blackwell Science Publications, Oxford, 376–462.

Cornford, C. 2011. *Training note*. Integrated Geochemical Interpretation Ltd, Bideford, UK.

Duan, Z.H., Moller, N. & Weare, J.N. 1992. An equation of state for the CH_4-CO_2-H_20 system: I. Pure systems from 0 to 1000 °C and 0 to 8000 bar. *Geochimica et Cosmochimica Acta*, **56**, 2605–2617.

Engelder, T. & Lacazette, A. 1990. Natural hydraulic fracturing. In: Barton, N. & Stephansson, O. (eds) *Rock Joints*. A. A. Balkema, Rotterdam, 35–44.

England, W.A., Mackenzie, A.S., Mann, D.M. & Quigley, T.M. 1987. The movement and entrapment of petroleum fluids in the subsurface. *Journal of Geological Society*, **144**, 327–347.

Fan, Z.Q., Jin, Z.-H. & Johnson, S.E. 2010. Subcritical propagation of an oil-filled penny-shaped crack during kerogen–oil conversion. *Geophysical Journal International*, **182**, 1141–1147.

Freiman, S.W. 1984. Effects of chemical environments on slow crack growth in glasses and ceramics. *Journal of Geophysical Research*, **89**, 4072–4076.

Freiman, S.W., Wiederhorn, S.M. & Mecholsky, J.J. Jr. 2009. Environmentally enhanced fracture of glass: a historical perspective. *Journal of the American Ceramic Society*, **92**, 1371–1382.

Guo, L.G., Xiao, X.M., Tian, H. & Song, Z.G. 2009. Distinguishing gases derived from oil cracking and kerogen maturation: Insights from laboratory pyrolysis experiments. *Organic Geochemistry*, **40**, 1074–1084.

Hantschel, T. & Kauerauf, A.I. 2009. *Fundamentals of Basin and Petroleum Systems Modeling*. Springer, New York, 151–169.

Horsfield, B., Schenk, H.J., Mills, N. & Welte, D.H. 1992. An investigation of the in-reservoir conversion of oil to gas: compositional and kinetic findings from closed-system programmed-temperature pyrolysis. *Organic Geochemistry*, **19**, 191–204.

Hunt, J.M. 1979. *Petroleum Geochemistry and Geology*. San Francisco, Freeman, 69–119.

Hunt, J.M. 1990. Generation and migration of petroleum from abnormally pressured fluid compartments. *American Association of Petroleum Geologists' Bulletin*, **74**, 1–12.

Jin, Z.-H. & Johnson, S.E. 2008. Primary oil migration through buoyancy-driven multiple fracture propagation: Oil velocity and flux. *Geophysical Research Letters*, **35**, L09303.

Jin, Z.-H., Johnson, S.E. & Fan, Z.Q. 2010. Subcritical propagation and coalescence of oil-filled cracks: Getting the oil out of low-permeability source rocks. *Geophysical Research Letters*, **37**, L01305.

Lacazette, A. & Engelder, T. 1992. Fluid-driven cyclic propagation of a joint in the Ithaca silstone, Appalachian Basin, New York. In: Evans, B. & Wong, T.-F. (eds) *Fault Mechanics and Transport Properties of Rocks*. Academic Press, London, 297–324.

Lash, G.G. & Engelder, T. 2005. An analysis of horizontal microcracking during catagenesis: Example from the Catskill delta complex. *American Association of Petroleum Geologists' Bulletin*, **89**, 1433–1449.

Lash, G.G. & Engelder, T. 2009. Tracking the burial and tectonic history of Devonian shale of the Appalachian Basin by analysis of joint intersection style. *Geological Society of America Bulletin*, **121**, 265–277.

Law, B.E. & Spencer, C.W. 1998. Abnormal pressure in hydrocarbon environments. In: Law, B.E., Ulmishek, G.F. & Slavin, V.I. (eds) *Abnormal Pressures in Hydrocarbon Environments*. American Association of Petroleum Geologists' Memoir, **70**, 1–11.

Lewan, M.D. & Roy, S. 2011. Role of water in hydrocarbon generation from Type-I kerogen in Mahogany oil shale of the Green River Formation. *Organic Geochemistry*, **42**, 31–41.

Luo, Q. 2010. Concept, principle, model and significance of the fault controlling hydrocarbon theory. *Petroleum Exploration and Development*, **37**, 316–324.

Luo, X.R. & Vasseur, G. 1996. Geopressuring mechanism of organic matter cracking: numerical modeling. *American Association of Petroleum Geologists' Bulletin*, **80**, 856–874.

Marquez, X.M. & Mountjoy, E.W. 1996. Microcracks due to overpressure caused by thermal cracking in well-sealed Upper Devonian reservoirs deep Alberta basin. *American Association of Petroleum Geologists' Bulletin*, **80**, 570–588.

Miller, T.W. 1995. New Insights On natural hydraulic fractures induced by abnormally high pore pressure. *American Association of Petroleum Geologists' Bulletin*, **79**, 1005–1018.

Nelson, R.A. 2001. *Geological Analysis of Naturally Fractured Reservoirs* (2nd edn). Gulf Professional Publishing, Butterworth-Heinmann, Boston, MA.

Nunn, J. 1996. Buoyancy-driven propagation of isolated fluid-filled fractures – implications for fluid transport in Gulf of Mexico geopressured sediments. *Journal of Geophysical Research*, **101**, 2963–2970.

Nunn, J. & Meulbroek, P. 2002. Kilometer-scale upward migration of hydrocarbons in geopressured sediments by buoyancy-driven propagation of methane-filled fractures. *American Association of Petroleum Geologists' Bulletin*. **86**, 907–918.

Olson, J.E. 1993. Joint pattern development – Effects of subcritical crack growth and mechanical crack interaction. *Journal of Geophysical Research*, **98**, 12 251–12 265.

Ozkaya, I. 1988. A simple analysis of oil-induced fracturing in sedimentary rocks. *Marine and Petroleum Geology*, **5**, 293–297.

Palciauskas, V.V. & Domenico, P.A. 1980. Microfracture development in compacting sediments: relations to hydrocarbon maturation kinetics. *American Association of Petroleum Geologists' Bulletin*, **64**, 927–937.

Pepper, A.S. & Dodd, T.A. 1995. Simple kinetic models of petroleum formation. Part II : oil-gas cracking. *Marine and Petroleum Geology*, **12**, 321–340.

Savalli, L. & Engelder, T. 2005. Mechnisms controlling rupture shape during subcritical growth of joints in layered rocks. *Geological Society of America Bulletin*, **117**, 436–449.

Stainforth, J.G. 2009. Practical kinetic modelling of petroleum generation and expulsion. *Marine and Petroleum Geology*, **26**, 552–572.

Tada, H., Paris, P.C. & Irwin, G.R. 2000. *The Stress Analysis of Cracks Handbook*. ASME Press, NY.

Tissot, B.P. & Welte, D.H. 1984. *Petroleum Formation and Occurrence, A New Approach to Oil and Gas Exploration*. Springer, Berlin, 276–298.

Tissot, B.P., Pelet, R. & Ungerer, P. 1987. Thermal history of sedimentary basins, maturation indices and kinetics of oil and gas generation. *American Association of Petroleum Geologists' Bulletin*, **71**, 1445–1466.

Vernik, L. 1994. Hydrocarbon generation induced microcracking of source rocks. *Geophysics*, **59**, 555–563.

Wang, Y.P., Wang, Z.Y., Zhao, C.Y., Wang, H.J., Liu, J.Z., Lu, J.L. & Liu, D.H. 2007. Kinetics of hydrocarbon gas generation from marine kerogen and oil: implications for the origin of natural gases in the Hetianhe gasfield, Tarim Basin, NW China. *Journal of Petroleum Geology*, **30**, 339–356.

Received 04 May 2011; revised typescript accepted 13 January 2012.